Geotextiles and Geomembranes xxx (xxxx) xxx

Contents lists available at ScienceDirect

Geotextiles and Geomembranes

journal homepage: www.elsevier.com/locate/geotexmem

Regular Paper

Effect of elevated temperatures on the degradation behaviour of elastomeric bituminous geomembranes

A. Samea [a], F.B. Abdelaal [b,*]

[a] GeoEngineering Centre at Queen's-RMC, Queen's University, Kingston, ON, K7L 3N6, Canada
[b] GeoEngineering Centre at Queen's-RMC, Queen's University, Ellis Hall, Kingston, ON, K7L 3N6, Canada

ARTICLE INFO

Keywords:
Geosynthetics
Bituminous geomembrane
Ageing
Thermo-oxidative degradation
Barrier systems

ABSTRACT

The effect of elevated temperatures on the degradation of an elastomeric bituminous geomembrane (BGM) when exposed to air and deionized (DI) water at temperatures between 22 and 85 °C is investigated using immersion tests. The changes in the mechanical, chemical and rheological properties of the BGM are examined over approximately two years under different ageing conditions. It is shown that the BGM exhibited different degradation rates in its different components when exposed to elevated temperatures that are dependent on the incubation media. In air, the BGM exhibited thermo-oxidative degradation in the elastomeric bituminous coat that changed the bitumen glass transition temperature and increased its rigidity. Further degradation led to the brittleness of the bitumen coat before any degradation in the tensile and puncture strengths of the BGM. In contrast, exposure to DI water resulted in faster degradation of the mechanical properties of the BGM, while the bitumen coat exhibited substantially less degradation than in air. Arrhenius modelling is used to estimate the degradation times of the BGM at a range of field temperatures for both media.

1. Introduction

Geomembranes are extensively used as part of the barrier systems in bottom liners and cover of different geoenvironmental applications to prevent the migration of liquids and gases to the surrounding environment. Most of these facilities are lined with polymeric geomembranes such as linear low-density polyethylene, high-density polyethylene, polyvinyl chloride, and polypropylene. This has led to extensive research targeting their short-term and long-term performances (especially for high-density polyethylene) over the last two decades (e.g., Abdelaal et al., 2014b; Abdelaal and Solanki 2022; Cazzuffi and Gioffrè 2020; Eldesouky and Brachman 2020; Marcotte and Fleming 2020; Müller, 2007; Rowe et al., 2020; Rowe and Sangam 2002; Rowe and Fan 2021, 2022; Scheirs 2009; Stark et al., 2020; Tian et al., 2018; Touze--Foltz et al., 2021; Vahidi et al., 2020). Bituminous geomembranes (BGMs) are also considered a strong candidate for the liner material in these applications due to their high puncture resistance, high mechanical properties, relatively high density, and low coefficient of thermal expansion (Peggs 2008). While historically the use of BGMs has been largely limited to dams, canals, and potable water reservoirs, more recently, they had been used to line mine tailings ponds, heap leach pads, and other geoenvironmental applications (Lazaro and Breul 2014; Peggs 2008). However, there is a paucity of research examining the long-term performance of BGMs in these different geoenvironmental applications. Additionally, there are no specifications to qualify the acceptance of BGMs for use in barrier systems of these geoenvironmental applications similar to those available for polymeric geomembranes (e.g., GRI-GM13, 2021). Thus, there is a need for extensive research into the long-term performance of BGMs to ensure their proper use in these applications to provide the desired environmental protection.

2. Background

BGMs are manufactured by impregnating a reinforcement layer typically comprising a nonwoven polyester geotextile (NW-GTX) and a glass fleece sheet with bitumen (Bannour et al., 2013). This reinforcement layer essentially provides the mechanical properties, while the bitumen provides the waterproofing properties of the BGM. Another bitumen layer is used as a tack coat to increase the geomembrane thickness and protect the impregnated reinforcement layers from thermal, UV, and chemical degradation during manufacturing and service (Daly and Breul 2017). The top surface of the BGM is typically sanded to

* Corresponding author.
E-mail addresses: alireza.samea@queensu.ca (A. Samea), fady.abdelaal@queensu.ca (F.B. Abdelaal).

https://doi.org/10.1016/j.geotexmem.2022.10.010
Received 3 April 2022; Received in revised form 18 October 2022; Accepted 20 October 2022

increase the interface friction between the BGM and the overlying liner materials, while the bottom side is bonded to a polymeric film to prevent the adhesion of the turns of the BGM roll during storage and potentially protect the BGM from upward root penetration during service (Lazaro and Breul 2014; Touze-Foltz and Farcas 2017). Due to the high sensitivity of the bitumen to temperature variations (Petersen 1998), oxidized (treated by blowing hot air) bitumen was historically used for the production of BGMs. Currently, most of the BGMs available in the market involve stabilized bitumen with elastomers such as Styrene-Butadiene-Styrene (SBS) copolymer (Scheirs 2009). These modifications increase the workable range of temperature of the bitumen by reducing the low-temperature brittleness and increasing its flow temperature ranges (Hunter et al., 2015; Touze-Foltz and Farcas 2017).

Many aspects of the performance of BGMs as the liner material in geoenvironmental applications rely on the characteristics of the bitumen (Touze-Foltz and Farcas 2017). As a mixture of oligomeric hydrocarbons, the bitumen typically comprises 80–88% carbon and 8–12% hydrogen with one or more nitrogen, sulfur, and oxygen heteroatoms (Lesueur 2009). This complex structure of the bitumen can be classified into four classes of compounds; saturates, aromatics, resins, and asphaltenes (SARA compounds; Aske et al., 2001; Corbett 1969; Ding et al., 2022; Hofko et al., 2017; Hunter et al., 2015; Masson and Polomark 2001). Previous studies (e.g., Corbett 1969; Dealy 1979; McKay et al., 1978; Sultana and Bhasin 2014; Wang et al., 2019b) showed that the rheological properties of bitumen are highly dependent on the SARA fractions. For example, these studies showed that increasing the asphaltene content (high polarity and molecular weight fractions) increases the stiffness and rigidity while increasing the other SARA components increases its viscosity. Thermo-oxidative degradation can alter the composition of these SARA fractions (e.g., increase the asphaltenes) that can change the ductility, glass transition temperature, and stiffness of the bitumen with time (e.g., Bachir et al., 2016; Fernández-Gómez et al., 2014; Lu and Isacsson 2002; Yu et al., 2014). Hence, investigating the changes in the bitumen composition or its chemical, mechanical, and rheological properties (that imply changes in its structure) can allow the assessment of their degradation (Hofko et al., 2017; Mouillet et al., 2011; Tauste et al., 2018; Touze-Foltz and Farcas 2017) and is essential to ensure the longevity of the BGM under field conditions.

Previous studies that investigated the durability of bitumen binders have focused on their photo and thermal degradations to assess the lifetime of asphalt pavements (e.g., Aguiar-Moya et al., 2017; Mouillet et al., 2011; Kaya et al., 2020; Lu et al., 2008). In the laboratory, these studies simulated thermal oxidation in the short-term using the rolling thin film test (RTFOT) by ageing the bitumen at 163 °C for 85 min. To simulate the long-term ageing conditions, the pressure ageing vessel (PAV) is used to age the bitumen at 100 °C under 2.1 MPa for 20 h (e.g., Lu and Isacsson 2002; Mirwald et al., 2020; Puello et al., 2013; Tauste et al., 2018). However, these test methods designated for pavements cannot simulate the aggressive long-term ageing conditions of the BGM liner in different geoenvironmental applications that differ from asphalt applications in terms of exposure to contaminants and elevated temperatures, longer required design life, and inaccessibility for repairs.

Attempts to investigate the long-term performance of BGMs in geoenvironmental applications have been limited to examining field exhumed samples. For instance, Addis et al. (2013) reported a failure of the BGM liner in a tailings storage facility after several months from installation and tailings deposition. Thermal imaging showed surface temperatures of the exposed BGM reaching 86.2 °C and the tensile tests conducted on exhumed samples revealed a decrease in the tensile strength, especially at the seamed BGM locations. Thus, the combination of the elevated temperatures and tensile stresses seemed to cause the BGM degradation and failure. Touze-Foltz and Farcas (2017) investigated the performance of elastomeric BGMs, aged for up to 30 years in water ponds at two different sites (with the average annual temperature ranging from 6.1 to 15.3 °C) in France. They showed that for the samples above the water line exposed for 30 years, the SBS copolymer was entirely consumed within the first microns from the surface, although it was still present at the core. Tensile test results showed that the mechanical properties of the core reinforcements were not affected after 30 years. It was concluded that after 30 years of exposure to water reservoir applications, the BGM maintained the same waterproofing characteristics as a virgin BGM. These two studies show how the service conditions, including the field temperature, can affect the service life of BGMs in geoenvironmental applications.

While these studies presented the first attempts to understand the performance of BGMs in the field for up to 30 years, extensive laboratory accelerating ageing studies are still needed to enable the understanding of their longer-term degradation behaviour and predict their longevity at field temperatures. This is essential to ensure that the BGM can provide adequate environmental protection during the design life of the different geoenvironmental applications that can range from decades to several centuries. Thus, the first objective of this study is to investigate the thermo-oxidative degradation of an elastomeric BGM at different temperatures when immersed in air and deionized (DI) water and its effect on the mechanical, chemical, and rheological properties of the BGM. The second objective is to use this data at elevated temperatures to predict the degradation in these properties at lower field temperatures using time-temperature superposition modelling.

3. Experimental investigation

3.1. Materials examined

The 4.8 mm thick BGM examined was manufactured with SBS modified bitumen and reinforced using a polyester NW-GTX and a glass fleece layer with mass per unit area of 275 and 50 g/m^2, respectively. Table 1 shows the initial properties of the BGM while Table 2 shows the initial properties of the NW-GTX used in the formulation of the BGM examined. In general, the initial mechanical properties of the BGM were different from those for NW-GTX given the different ASTM index tests designated for assessing their initial properties with different sample sizes and loading rates.

Table 1
BGM initial properties (mean ± standard deviation).

Property[a]	Method	*BGM*[b]
Designator	–	TERANAP 531 TP 4M
Nominal Thickness (mm)	ASTM D5199	4.8 ± 0.120 (4.6)
Mass Per Unit Area of the Glass fleece Reinforcement (g/m^2)	–	50[a]
Mass Per Unit Area of the Nonwoven Geotextile Reinforcement (g/m^2)	ASTM D5261	275[a]
Mass Per Unit Area of the BGM (g/m^2)	ASTM D5261	5410[c]
Machine Direction Maximum Tensile Strength (kN/m)	ASTM D7275	33.1 ± 0.422 (25.5)
Machine Direction Elongation at Maximum Tensile Strength (mm)	ASTM D7275	51 ± 1.8 (33)
Cross Machine Maximum Tensile Strength (kN/m)	ASTM D7275	29.5 ± 0.887 (23)
Cross Machine Elongation at Maximum Tensile Strength (mm)	ASTM D7275	52 ± 1.5 (35.7)
Puncture Resistance (N)	ASTM D4833	690 ± 41.91 (555)
Puncture Elongation at Puncture Resistance (mm)	ASTM D4833	14.35 ± 0.933
Glass Transition Temperature (of the Bitumen Tack Coat) (°C)	ASTM E2602	−24.2 ± 1.48

[a] 10 replicates were examined for each property.
[b] Values in parentheses show the minimum specified value by the manufacturer for this BGM.
[c] Values from the manufacturer datasheet.

Table 2
NW-GTX initial properties (mean ± standard deviation).

Property[a]	Method	NW-GTX
Nominal Thickness (mm)	ASTM D5199	1.1 ± 0.128
Surface Mass Per Unit Area (g/m²)	ASTM D5261	263 ± 4.36
Machine Direction Maximum Tensile Strength (kN/m)	ASTM D5035	13.4 ± 1.33
Machine Direction Elongation at Maximum Tensile Strength (mm)	ASTM D5035	48 ± 3.7
Cross Machine Maximum Tensile Strength (kN/m)	ASTM D5035	10.5 ± 0.866
Cross Machine Elongation at Maximum Tensile Strength (mm)	ASTM D5035	55 ± 1.2
Puncture Resistance (N)	ASTM D4833	627 ± 62.37
Puncture (Break) Elongation	ASTM D4833	16.79 ± 0.665
Glass Transition Temperature (°C)	ASTM E2602	82.86 ± 2.27

[a] 10 replicates were examined for each property.

Table 3
Chemical constituents of DI water used in this study (mg/l except for pH and Langelier Index).

Analyte	DI water
pH	~6.5
Langelier Index (25 °C)[a]	−2.5
Aluminum	<1.0
Ammonium	–
Calcium	<0.05
Cobalt	<0.02
Copper	<0.2
Iron	<0.05
Magnesium	<0.05
Manganese	<0.05
Nickel	<0.3
Potassium	<0.2
Sodium	<1.0
Sulfur	<1.0
Zinc	<0.01
Chloride	<0.5
Sulphate	<0.1

[b]Calculated according to Benefield et al. (1982).

3.2. Accelerating ageing method

Jar immersion technique (coupons of the geomembrane immersed in a jar filled with a synthetic solution and separated using glass rods) is typically used to accelerate the ageing of geomembranes in the laboratory at elevated temperatures (e.g., Abdelaal et al., 2019; Ewais et al., 2014, 2018; Hsuan and Koerner 1998; Müller and Jacob 2003; Rowe and Ewais 2014). Since the stresses on the liner and the composite liner exposure conditions cannot be simulated in these tests, the service life of the geomembrane that is related to the loss of its hydraulic barrier function (i.e., time to rupture) cannot be directly estimated from immersion tests. However, these tests can be used to assess the degradation times in the different properties of the geomembrane until the nominal failure of the material is reached. Time to nominal failure for geosynthetics is typically assessed as the time taken for a geomembrane property to decrease to 50% of the initial or the specified value (Hsuan and Koerner 1998; Rowe et al., 2009) and hence it can be used to examine the effects of the field exposure conditions on the chemical durability of the geomembrane.

Due to the multi-component nature of the BGMs, cutting small coupons from the roll in immersion tests can directly expose the core NW-GTX to the solutions that can affect their overall degradation (Samea and Abdelaal 2019). While this can occur at certain locations of the liner in the field (e.g., seams), the core NW-GTX will not be directly exposed to the solution in most of the area of the BGM liner in the field. Thus, in this study, the 250 × 150 mm coupons of the BGM were cut and sealed using BGM strips that were seamed to the four edges of the coupon to ensure the BGM is exposed to the solution from the top (bitumen coat) and bottom (polymeric film) surfaces only (Samea and Abdelaal 2019). The sealed coupons were then incubated in stainless steel containers at different elevated temperatures.

Air and DI water (Table 3) were selected as the immersion media to investigate the effect of elevated temperatures on the long-term performance of BGMs. This is because air and DI water immersion allow exploring the effect of elevated temperatures on the durability of BGMs without the other complicating factors that arise from incubation in complex synthetic solutions such as the reactions between the different chemicals, salt precipitation, or reactions of the chemicals with the bitumen. The BGM coupons were incubated at 40, 55, 70 and 85 °C in air, while in DI water, the immersion was conducted at room temperature (≈22 °C), 40, 55 and 70 °C with a surface area of BGMs per solution volume of 450 cm^2/L 85 °C was not used for DI water immersion since it was close to the softening point of bitumen and hence it was not possible to vertically place the BGM coupons in the containers. Additionally, the NW-GTX reinforcement used in the formulation of the BGM examined was incubated in DI water at room, 40, 55 and 70 °C to compare the degradation of the NW-GTX to the overall degradation of the BGM. The DI water was replaced every two months for both BGM and NW-GTX during the testing period.

3.3. Index testing

Different index tests were used to examine the changes in the mechanical, chemical, and rheological properties of the BGM due to chemical degradation using the samples obtained from the immersion tests at different incubation times and temperatures. Ten different specimens were examined to assess the initial properties of the BGM, whereas lower number of specimens was examined at different incubation times to ensure the availability of samples during the entire duration of the long-term study. For the degradation in the bitumen coat, while it is expected that the degradation varies with the depth from the exposed surface (Touze-Foltz and Farcas 2017), in this study the chemical and rheological properties were assessed for the entire thickness of the bitumen coat to assess the average degradation across the bitumen thickness in these properties with time.

3.3.1. Mechanical index tests

The tensile and puncture tests were conducted to monitor the effect of ageing on the mechanical properties of the BGM and the core NW-GTX. Due to the relatively large size of the specimens, only one specimen for puncture and two specimens for tensile were examined at different temperatures to assess the degradation of the mechanical properties of the aged BGM with time. The tensile tests were conducted using a Zwick Roell universal testing machine (Model Z020) according to ASTM D7275. A 50 mm/min strain rate was applied to the BGM until rupture and the maximum stress and the corresponding elongation were recorded (ASTM D7275). Similarly, the tensile properties of the core NW-GTX were investigated using the ASTM D5035 test method at a strain rate of 300 mm/min. The puncture resistance of the BGM and the NW-GTX samples were measured using a GDS loading machine according to the modified ASTM D4833/D4833M method at a strain rate of 50 mm/min. The maximum force and corresponding elongation were recorded as the index static puncture resistance. The maximum stresses and corresponding elongations were used in this study for both the tensile and puncture properties instead of the break stress and elongation because they represent the onset of the NW-GTX failure that governs the mechanical properties of the BGM. This also allows the comparison of the degradation in the mechanical properties of the BGM to the NW-GTX samples that were separately incubated under the same conditions.

3.3.2. Chemical and rheology index tests

3.3.2.1. Modulated differential scanning calorimetry. In the asphalt research, the glass transition temperature (T_g) is typically used as an indicator of the degradation of bitumen when exposed to service conditions (Kaya et al., 2020; Mark et al., 2004; Puello et al., 2013; Yu et al., 2019). In amorphous or random network materials, T_g refers to the energy needed to break and recreate covalent bonds (Ojovan 2008) that separates between the glass-like brittle behaviour below T_g and the rubbery-like behaviour above T_g (Aguiar-Moya et al., 2017; Kriz et al., 2007). Ageing can alter the thermal characteristics of polymer-modified bitumen, and hence its T_g due to changes in the chemical structure of the bitumen (Kaya et al., 2020; Wang et al., 2019a).

In this study, a TA Instruments Modulated Differential Scanning Calorimetry (MDSC250) equipped with a refrigerated cooling system (RCS120) was used to investigate the average effect of ageing on the T_g of the bitumen tack coat according to ASTM E2602 test method. The MDSC was used instead of conventional DSCs due to its capability to separate overlapped reversing and non-reversing thermal events that occur at the same temperature range such as those involved in glass transition events (Masson and Polomark 2001; Verdonck 2010). Bore-cut specimens were initially extracted from the aged or unaged BGM samples, then 5–8 mg of the top layer of the specimen only involving the bitumen coat was cut and placed in Tzero hermetic pans with hermetic lids. The sealed pans were examined in the MDSC under a constant flow (50 mL/min) of nitrogen and heated to 170 °C and then quenched to −110 °C at a rate of 10 °C/min. Then, the samples were reheated to 170 °C at a rate of 5 °C/min while the temperature was modulated with an amplitude of ±0.75 °C and a period of 1 cycle/min. For the aged BGM samples, three different specimens were examined for each data point to assess the change in the T_g values that reflects the average effect of ageing on the entire thickness of the tack coat bitumen only.

3.3.2.2. Dynamic shear rheometer. An Anton Paar MCR102 Dynamic Shear Rheometer (DSR) was used to assess the effect of ageing on the rheological properties of the BGMs samples at different temperatures. Linear amplitude sweep tests were performed with a fixed angular frequency of 10 rad/s, 1 N normal force, and 0.01%–60% strain values using a 25 mm spindle to explore the changes with time in the complex shear modulus (G^*) and the phase angle (δ) of the BGM. G^* is defined as the ratio of the absolute shear stress and the resulting shear strain while δ is the offset between the applied shear stress and resulting shear strain from a dynamic oscillation measurement that can be used to characterize the viscous and elastic behaviour of the bitumen (Airey 2003). Three aged BGM specimens were examined for each data point in the DSR at a constant temperature of 55 °C to remove the potential effects of the test temperature on the results and to monitor the changes in G^* and δ of the BGM with ageing at different temperatures. Both G^* and δ were measured in the linear viscoelastic region (LVE) since their values remain constant at such relatively low strains (Omairey et al., 2020).

3.3.2.3. Fourier transform infrared spectroscopy. Fourier Transform Infrared Spectroscopy (FTIR) technique provides information on the functional groups of elastomeric bitumen (Fig. 1) that change with ageing and hence, can be used to explore the average degradation in the bitumen and the SBS copolymer in the bitumen top coat (Aguiar-Moya et al., 2017; Durrieu et al., 2007). A solution prepared from the whole thickness of the bitumen coat comprising 10% bitumen by mass dissolved in toluene, was used to prepare the samples for the FTIR tests (Arias, 2019; Zeng et al., 2015) to minimize the possibility of having any NW-GTX fibres and sand particles in the bitumen sample. The solution was dried on a potassium bromide (KBr) disk and four specimens were prepared for each data point. The specimens were tested using a Thermo Scientific Nicolet iS20 spectrum to scan the functional groups in the range of 400–4000 cm^{-1} with a frequency of 32 and at a resolution of 4 cm^{-1}.

To study the effect of ageing on the functional groups of the bitumen and SBS copolymer, changes in the carbonyl C═O and the butadiene double bonds C═C characteristic bands were monitored at different incubation times. The C═O (centered around 1700 cm^{-1}) band was used to monitor the oxidation of the entire bitumen coat, whereas the C═C (centered around 968 cm^{-1}) band was used to monitor the degradation of the chain segments in the butadiene phase of the SBS. The carbonyl and butadiene indices were calculated using the band areas from valley to valley method (e.g., Lamontagne et al., 2001; Mouillet et al., 2008; Zeng et al., 2015) viz:

$$I_{C=O} = \frac{A_{C=O}}{\sum \text{Area}} \quad \text{(Eq 1)}$$

$$I_{SBS} = \frac{A_{SBS}}{\sum \text{Area}} \quad \text{(Eq 2)}$$

Where; $I_{C=O}$ = carbonyl index, $ISBS$ = butadiene index, $A_{C=O}$ = Area of the carbonyl band centered around 1700 cm^{-1}, A_{SBS} = Area of the butadiene band centered around 968 cm^{-1}, and ΣArea = summation of the areas of the spectral bands between 4000 and 600 cm^{-1}.

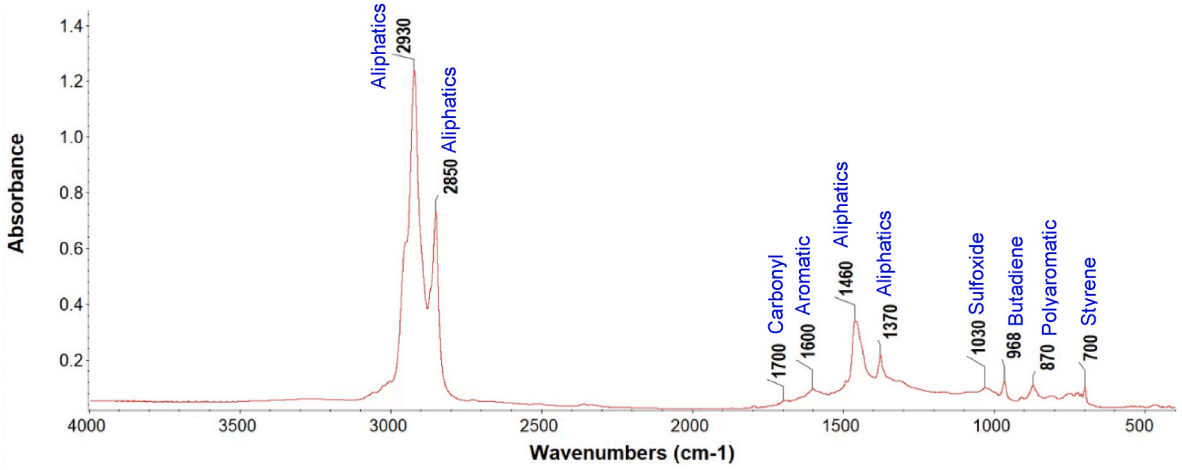

Fig. 1. FTIR spectrum of control bitumen sample (unaged) with approximate wavenumbers and the corresponding compounds relevant to the SBS modified bitumen.

4. Results and discussion

4.1. Effect of incubation media on the mechanical properties of BGM at 70 °C

The BGM samples immersed in air and DI water at 70 °C showed different degradation behaviour in their mechanical properties (Figs. 2 and 3). In DI water, the mechanical strengths of the BGM assessed in terms of the maximum (peak) tensile stress and force at puncture were retained at the initial values for the first 4 months. Then, the values linearly decreased to reach approximately 10–20% of the initial values after around 15 months from the start of incubation to stabilize at this value until the end of the incubation duration of 27 months. In air, no measurable changes in the tensile and puncture strengths were observed until the end of the incubation duration of 29 months (Fig. 2).

For the tensile and puncture elongations measured at the maximum (peak) stress/force (ε_{max}), the values decreased with time after incubation in air and DI water at 70 °C (Fig. 3). For the tensile tests, ε_{max} decreased after incubation in DI water to reach 10% of the initial values after around 18 months, then stabilized at this value until the end of the incubation. For ε_{max} from the puncture test, the values linearly decreased to reach 50% of the initial value after 14 months, at which it was stabilized until the end of incubation. In air, ε_{max} from the tensile and puncture tests decreased with time to reach 60% of the initial values after 29 months and hence showing slower degradation than in DI water.

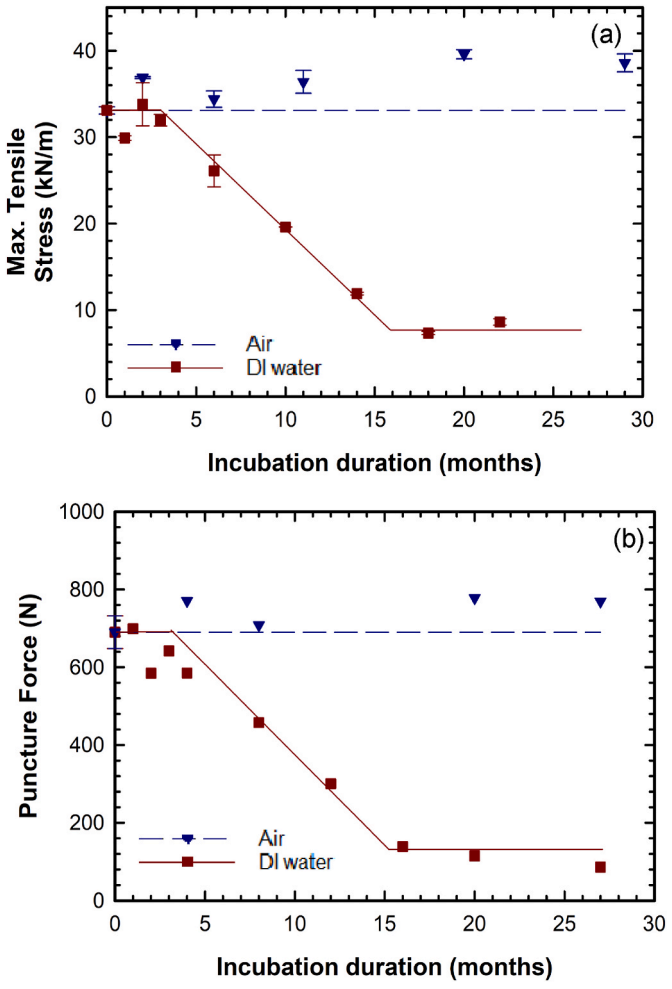

Fig. 2. Variation with incubation time at 70 °C in air and DI water in (a) machine direction tensile peak stress; and (b) peak puncture force.
(Note: unless otherwise noted, the data points presented in all the figures represent the mean value, while the error bars represent the ± 1 standard deviation of the data).

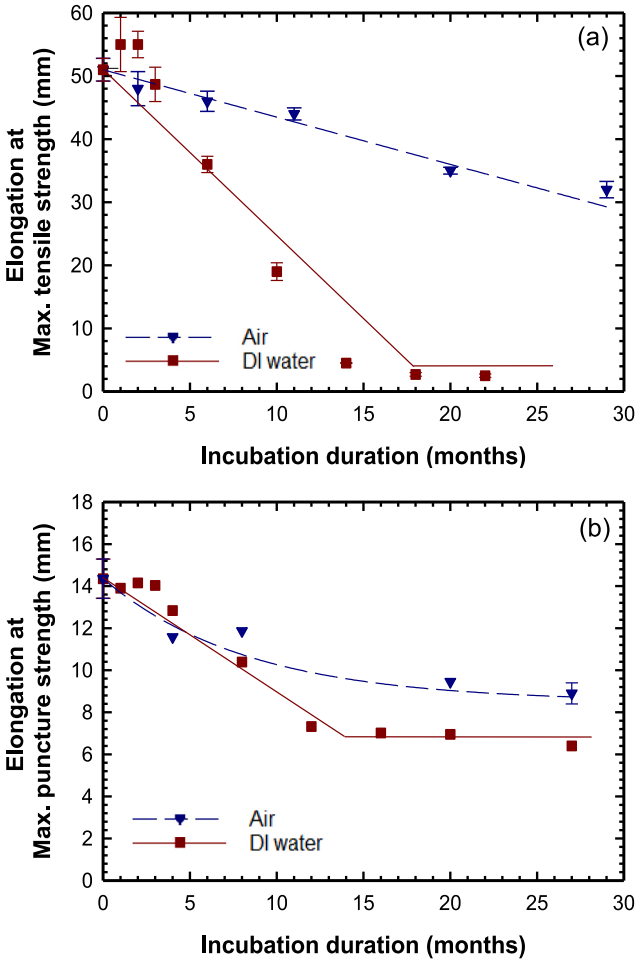

Fig. 3. Variation with incubation time at 70 °C in air and DI water in (a) machine direction elongation at peak tensile stress; and (b) elongation at peak puncture force.

Although all the mechanical properties revealed faster degradation in DI water than in air, samples immersed in air started to show signs of brittleness in the bitumen coat after 22 months of incubation at 70 °C, while the DI water samples did not show any brittleness during the entire 27 months of incubation. The brittleness in the BGM samples was evidenced by the surface cracks developed in the bitumen tack coat only (i.e., did not propagate through the entire BGM thickness) when they were bent by hand or during the mechanical tests shortly after loading (Fig. 4). However, the values of the maximum stresses and corresponding elongations obtained for the BGM samples after 22 months in air were still higher than those obtained from the DI water samples at similar incubation times. This suggests that the brittleness in the bitumen coat had less effect on the mechanical properties than the degradaion of the BGM in DI water.

4.2. Effect of incubation media on the chemical and rheological properties of the BGM at 70 °C

4.2.1. Glass transition temperature

In both air and DI water, there was a decrease in the T_g values with the incubation time (Fig. 5). In air, the T_g of the unaged bitumen of −24.2 °C decreased upon incubation over the first 9 months to reach −37 °C then stabilized at this value until the end of the incubation duration. In DI water, T_g was retained at the initial values for the first 7

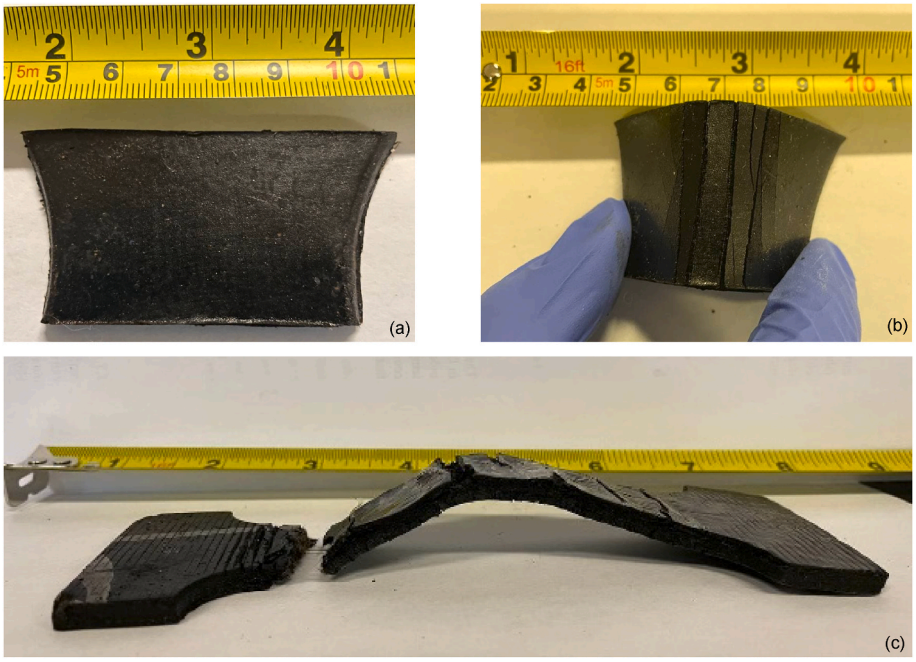

Fig. 4. Photographs of the samples aged in air at 70 °C after 22 months: (a) samples taken out of the oven; (b) samples after bending by hand; (c) cracks in the bitumen coat after the tensile test.

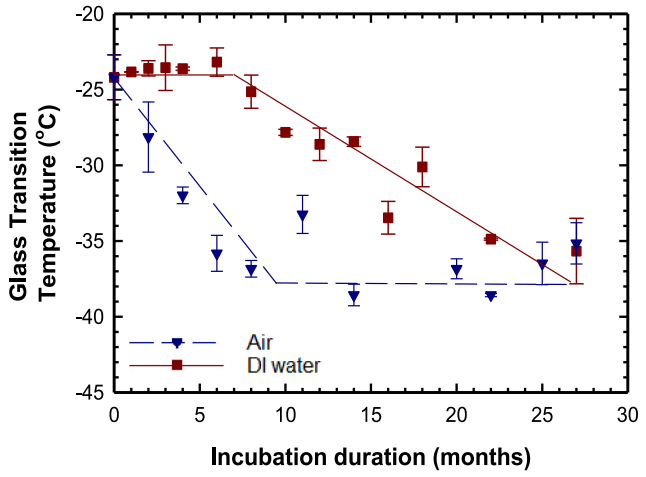

Fig. 5. Variation in glass transition temperature with incubation time at 70 °C in air and DI water.

months then decreased linearly to reach −37 °C at 27 months. Although similar T_g values were reached at the end of incubation in air and DI water, the faster decrease in T_g in air suggests that the change in the bitumen structure and composition due to thermo-oxidation degradation was faster than in DI water at 70 °C.

4.2.2. Complex shear modulus and phase angle

Using the linear amplitude sweep test, G^* and δ were monitored for the samples incubated in air and DI water as indicators of the changes in the viscoelastic characteristics of the BGM. The initial G^* of the unaged BGM was around 112 kPa, while the initial δ was around 43° implying similar proportions of the viscous and elastic structures of the unaged BGM (Hunter et al., 2015). After immersion in air at 70 °C, G^* started to increase whereas δ decreased during the 27 months of incubation (Fig. 6). Similar changes in G^* and δ were measured for the samples incubated in DI water but at slower rates. After 27 months of incubation, the G^* of the samples immersed in air was around four times higher than those incubated in DI water, whereas the δ was 1.5 times lower than those incubated in DI water. This increase in G^* and reduction in δ due to ageing show that the thermo-oxidative degradation shifted the bitumen toward the elastic behaviour (i.e., less viscous and more solid-like behaviour). This can be attributed to the oxidation of the bitumen and

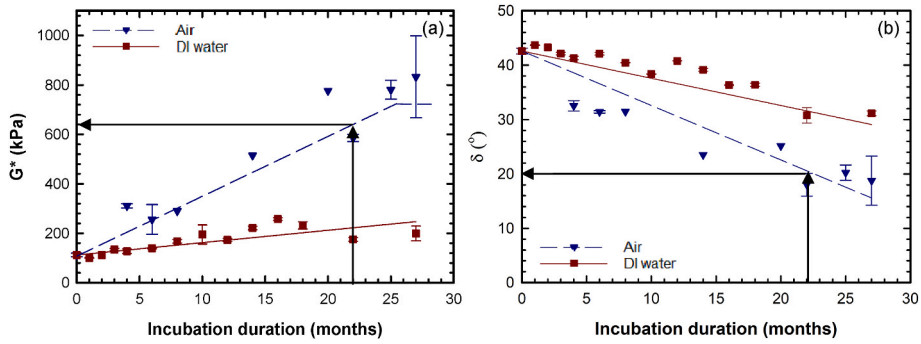

Fig. 6. Variation with incubation time at 70 °C in air and DI water in (a) complex shear modulus; (b) phase angle. Arrows represent the values at which the air immersed samples reached brittleness.

the volatilization of the lighter components such as the saturates and aromatics during ageing at elevated temperatures (Zhang et al., 2020).

4.2.3. Carbonyl and SBS indices

Incubation in air and DI water increased the $I_{C=O}$ of the unaged bitumen (0.0024) with time due to oxidative degradation, while the I_{SBS} was reduced inferring a degradation by chain scissioning of the butadiene segments (Touze--Foltz and Farcas 2017) (Fig. 7). After 27 months, the $I_{C=O}$ of samples immersed in air was 18 times higher than the initial value, while in DI water it was only increased by a factor of 6. Similarly, more reduction in the I_{SBS} was measured for the air immersed samples by the end of the incubation reaching around 55% of the initial value versus a reduction to only 80% of the initial value for the samples immersed in DI water. Thus, similar to T_g, G^*, and δ, the higher changes in the carbonyl and SBS indices for the samples incubated in air show that the degradation of the elastomeric bitumen coat was faster than in DI water.

4.3. Discussion of BGM ageing mechanism at elevated temperatures

Exposure of the BGM to elevated temperatures in either air or DI water led to changes in the chemical properties of the bitumen coat. Thermo-oxidative degradation resulted in an increase in the oxygenated compounds and deterioration of the SBS copolymer evidenced by the increase in $I_{C=O}$ and decrease in the I_{SBS}, respectively. As the structure and composition of the bitumen change with ageing, there was a change in the T_g of the bitumen. This can be attributed to the decrease in the T_g of the SARA compounds (specifically the saturates) with ageing shifting the overall T_g of the bitumen to lower temperatures (Kaya et al., 2020). Thermo-oxidative degradation also led to the increase in the rigidity of the bitumen due to the loss of the viscous fractions of its structure and hence G^* increased while δ was reduced. Further degradation can result in the embrittlement and cracking of the bitumen attributed to degradation by crosslinking of the bitumen molecules (Airey 2003; Jing et al., 2019; Mouillet et al., 2011; Omairey et al., 2020; Zeng et al., 2015).

In air, oxidative degradation of the bitumen coat was faster than in DI water resulting in the brittleness observed after 22 months of incubation at 70 °C. The measured values of T_g, $I_{C=O}$, I_{SBS}, G^*, and δ at the first time brittleness was observed in the aged samples were −37 °C, 0.035, 0.0095, 640 kPa, and 20°, respectively. This shows a 52% decrease in T_g, 1300% increase in $I_{C=O}$, 33% decrease in I_{SBS}, 470% increase in G^*, and 53% decrease in δ. While these values show excessive degradation in the chemical and rheological properties of the bitumen, the BGM retained its unaged mechanical strength but showed a reduction in ε_{max} with ageing. These changes in ε_{max} of the BGM in air can be attributed to the increase in the bitumen rigidity/stiffness that is implied by the changes in the values of G^* and δ due to ageing (Liu et al., 2003). This resulted in an increase in the overall stiffness of the BGM that led to the fast increase in the stresses after loading the aged samples in the mechanical tests to reach the unaged peak strength but at relatively low elongations. With the increase in the bitumen rigidity due to ageing in air, the stiffness of the BGM increased and hence ε_{max} decreased with time (Fig. 8a). Thus, while the NW-GTX may have not exhibited noticeable thermo-oxidative degradation in air, the increase in the rigidity of the bitumen coat is hypothesized to decrease the ductility of the BGM but not its strength.

After 27 months of incubation in DI water at 70 °C, the measured values of T_g, $I_{C=O}$, I_{SBS}, G^*, and δ were −37 °C, 0.015, 0.0114, 200 kPa, and 31°, respectively. While these values reflect lower changes in the

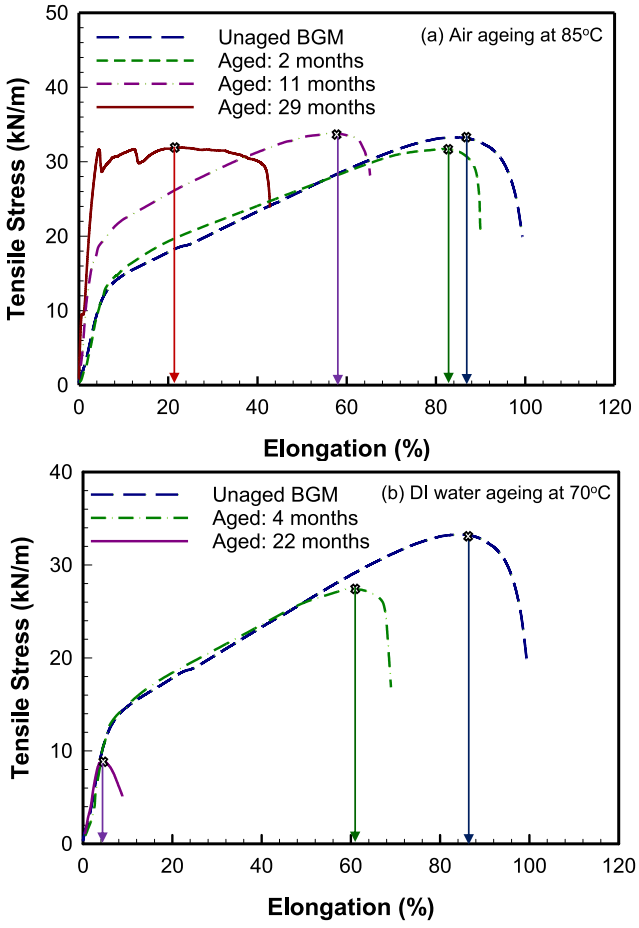

Fig. 8. Tensile stress versus elongation for: (a) aged BGM in air at 85 °C for 2, 11, and 29 months (11- and 29-months aged samples are with brittle bitumen coat); (b) aged BGM in DI water at 70 °C for 4 and 22 months. Arrows show the elongations at maximum stresses (ε_{max}).

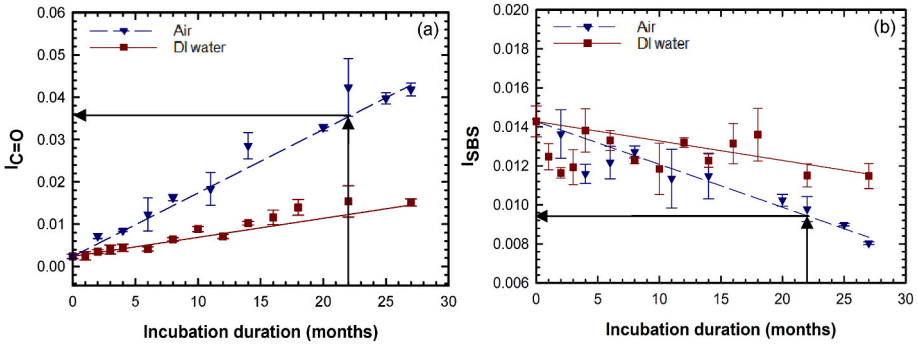

Fig. 7. Variation with incubation time at 70 °C in air and DI water in (a) $I_{C=o}$; (b) I_{SBS}. Arrows represent the values at which the air immersed samples reached brittleness.

chemical and rheological characteristics of the bitumen coat than those measured in air, the BGM showed faster degradation in its strengths and ε_{max} than in air (Fig. 8b). This suggests that the degradation in the mechanical properties of BGM in DI water could be due to the degradation of the NW-GTX, given the insignificant contribution of the polymeric film to the mechanical properties. The fast degradation of the NW-GTX in DI water can be attributed to the hydrolysis of the polyester fibres when the hydrogen (H^+) or hydroxide (OH^-) ions attack their long-chain linear molecules (Dumitru et al., 2017; Elias et al., 1998; Mathur et al., 1994). Although the bitumen coat is expected to protect the NW-GTX from degradation, the similar degradation in all the mechanical properties of the BGM and the NW-GTX that was separately examined in DI water (Fig. 9) suggest that the H^+ or OH^- ions can readily diffuse into the relatively intact/slightly degraded bitumen coat. This may have resulted in such fast degradation of the mechanical properties of the BGM in DI water.

The ageing results at 70 °C show the different degradation behaviours of BGMs in different incubation media (i.e., air and DI water). Due to their multi-component nature, these results also highlight the importance of establishing the degradation behaviour of BGMs based on the holistic investigation of their chemical, mechanical, and rheological properties. This is because the BGM can exhibit different degradation rates in its different components and hence different properties are required to assess their degradation. In this case, nominal failure of the BGM as a liner material can be defined as the time taken for the bitumen coat to lose its viscoelastic characteristics or for the BGM to reach 50% of its initial or specified mechanical properties. This shall allow assessing the BGM durability considering the different degradation mechanisms and rates in its different components to provide reliable estimates of their long-term performance for different exposure conditions.

4.4. Effect of incubation temperature on the mechanical properties of BGM

Due to the availability of more data from the tensile test than the puncture test at different temperatures, in this paper the tensile properties were only used to investigate the degradation of the BGM samples at different temperatures (40, 55, 70, and 85 °C in air and 22, 40, 55, and 70 °C in DI water). In air, the tensile strength did not change during the 29 months of exposure even at the highest temperature of 85 °C (Fig. 10a). However, ε_{max} decreased at temperatures between 55 °C and 85 °C to reach 80% of the initial value at 55 °C, 60% of the initial value at 70 °C, and 25% of the initial value at 85 °C after 29 months (Fig. 10c). Similar to 70 °C, brittleness in the bitumen coat was observed for the 85 °C samples but after 7 months from incubation while the BGM strength was retained at the unaged values and the ε_{max} was at around 80% of the initial value.

In DI water, the decrease in tensile strength was only observed at 70 °C while the values at temperatures at and below 55 °C were retained at the initial values (Fig. 10b). For the ε_{max}, the BGM exhibited degradation at 55 °C to reach 80% of the initial values after around 22 months of incubation (Fig. 10d). Thus, the degradation in mechanical properties was faster in DI water than in air at all temperatures due to the degradation of the polyester NW-GTX by hydrolysis in DI water that affected the mechanical properties of the BGM.

4.5. Effect of incubation temperature on the chemical and rheological properties of BGM

4.5.1. Glass transition temperature

In both air and DI water, T_g of the bitumen coat decreased with increasing the incubation time and increasing the immersion temperature as a result of the higher degree of thermo-oxidative degradation (Fig. 11). In air, the T_g of the BGM samples changed upon the incubation of the samples at all incubation temperatures between 40 and 85 °C. At 70 and 85 °C, T_g decreased to reach −37 °C after 9 and 4 months, respectively and further incubation did not show any change in the values. This plateau value in T_g was reached even before brittleness in the bitumen coat was observed after 22 and 7 months at 70 and 85 °C, respectively. For DI water, slower changes were observed only at 55 and 70 °C following a retention period at the unaged values of around 7 months after incubation. The T_g results at different temperatures show that exposure to air can alter the bitumen structure and hence change its T_g faster than in DI water even at temperatures as low as 40 °C.

4.5.2. Complex shear modulus and phase angle

Similar to T_g, the changes in the rheological properties of the bitumen in air were higher than in DI water at all incubation

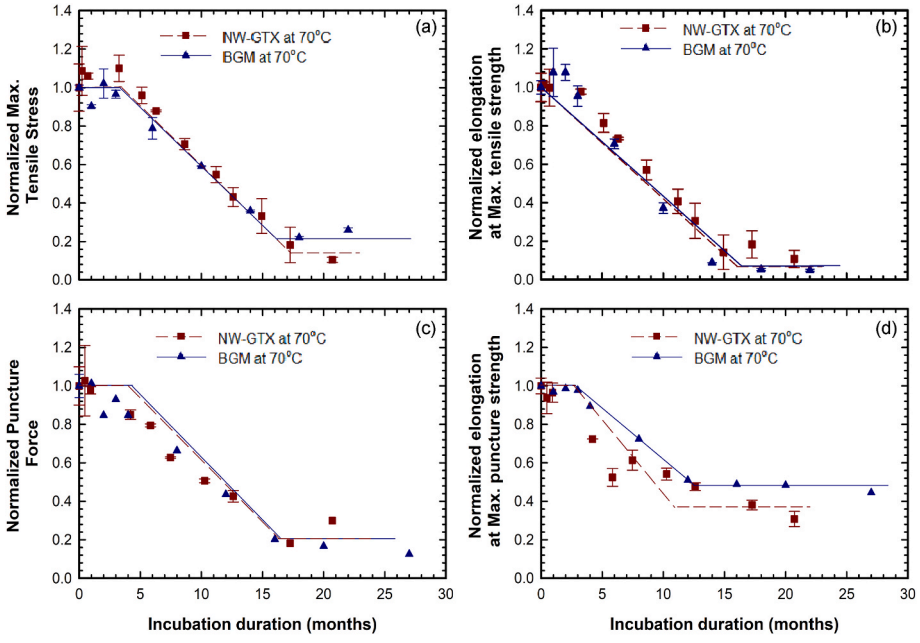

Fig. 9. Variation with incubation time for the BGM and the NW-GTX in DI water at 70 °C in the normalized values (aged values/initial values) of the (a) maximum tensile stress; (b) elongation at maximum tensile stress; (c) peak puncture force; (d) elongation at peak tensile force.

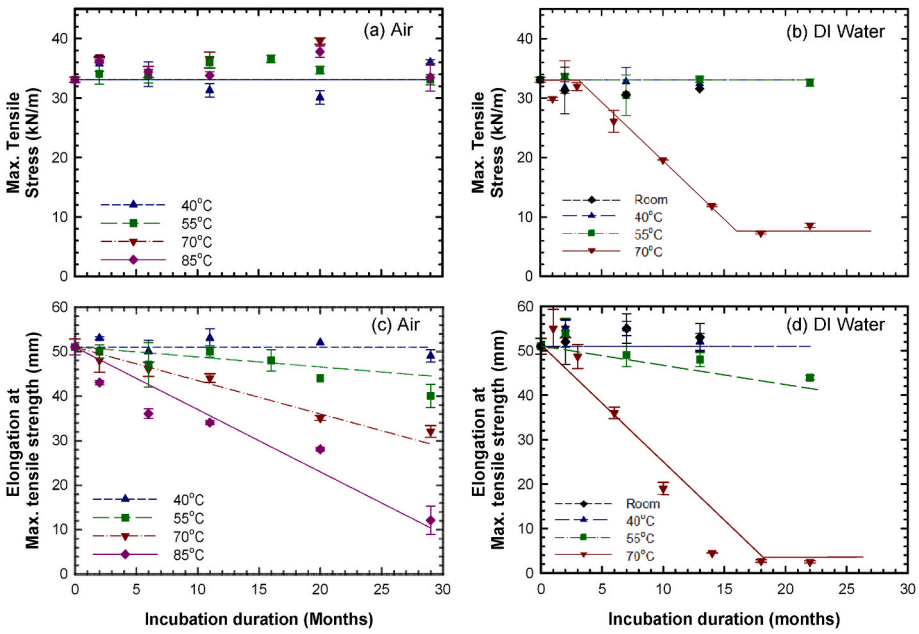

Fig. 10. Variation in tensile properties in machine direction with incubation time at different temperatures for (a) maximum tensile stress in air; (b) maximum tensile stress in DI water; (c) elongation at maximum tensile stress in air; (d) elongation at maximum tensile stress in DI water.

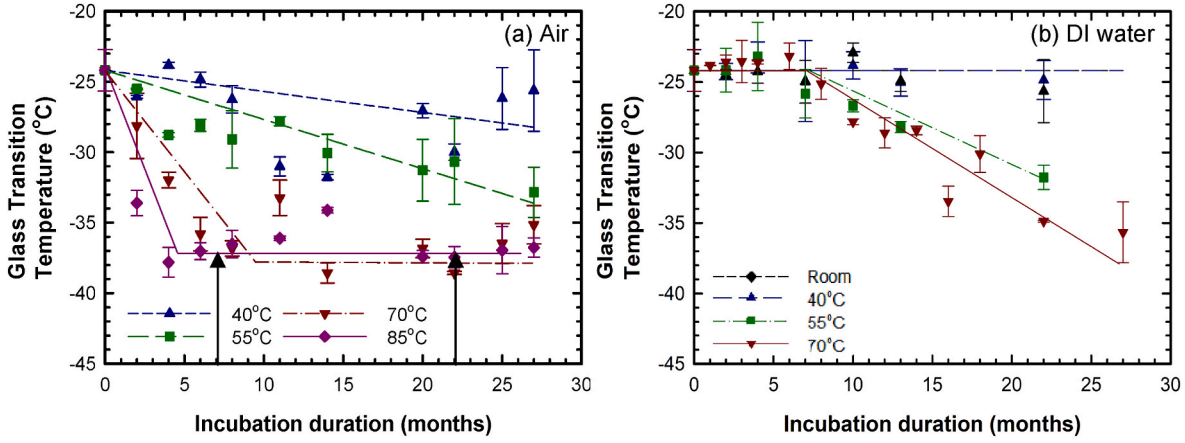

Fig. 11. Variation in glass transition temperature with incubation time in (a) air; (b) DI water. Arrows represent the values at which the air samples reached brittleness at 70 and 85 °C.

temperatures (Fig. 12). In air at 70 and 85 °C, a similar plateau value of G^* of around 720 kPa was reached after 25 and 8 months, respectively, and the values of G^* were scattered around this value until the end of incubation at the two incubation temperatures. Likewise, δ dropped to about 80% of the initial value after 10 months at 85 °C and then stabilized at this value until the end of the incubation duration, while at 55 and 70 °C, the values were still decreasing until the end of incubation. At 85 °C, the values of G^* and δ at the time of brittleness of the bitumen coat (i.e., after 7 months) were around 640 kPa and 20°, respectively, that were similar to values obtained at 70 °C at brittleness. While these values reflect a substantial change in the bitumen rigidity (i.e., at brittleness), G^* and δ exhibited further changes until the plateau values were reached suggesting that the bitumen underwent further changes in its rheology after the brittleness was first observed.

4.5.3. Carbonyl and SBS indices

The FTIR results presented in terms of the $I_{C=O}$ and the I_{SBS} obtained at different temperatures showed that the oxidation of bitumen and deterioration of the SBS copolymer were occurring concurrently (Fig. 13). For instance, in air, at 85 °C, the $I_{C=O}$ increased by a factor of 27 after 14 months of incubation and the data points were scattered around this value until the end of incubation. The I_{SBS} was also reduced by a factor of 10 after around 18 months and was stabilized at this value until 27 months. For the air immersed samples, brittleness in the bitumen coat was observed before the plateau values of both indices were reached at 85 °C (i.e., after 7 months) and at similar values to those observed at 70 °C but after 22 months of incubation. Thus, similar to results obtained for G^* and δ, this suggests that the bitumen exhibited further degradation after the time at which the early signs of brittleness were observed at 70 and 85 °C. Overall, both indices showed measurable degradation in the different components of the elastomeric bitumen (i.e., the bitumen and the SBS copolymer) at temperatures as low as 55 °C in both air and DI water but slight degradation at 40 °C.

4.6. Arrhenius modelling and predictions of the time to nominal failure

The degradation rates obtained for the BGM samples immersed in air and DI water at different temperatures were used to establish predictions

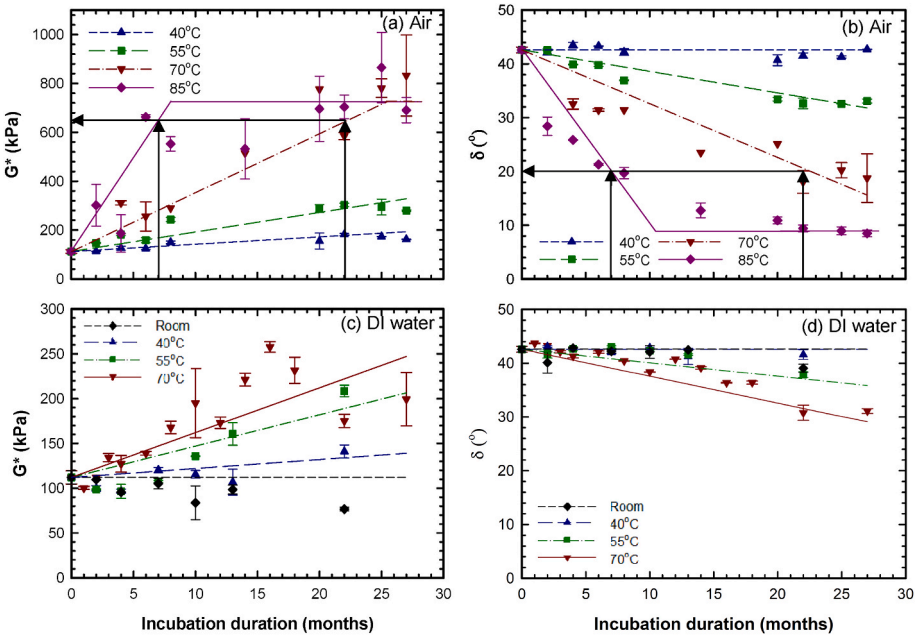

Fig. 12. Variation of the rheological properties with the incubation time of the BGM at different temperatures: (a) complex shear modulus in air; (b) phase angle in air; (c) complex shear modulus in DI water; (d) phase angle in DI water. Arrows represent the values at which the air samples reached brittleness at 70 and 85 °C.

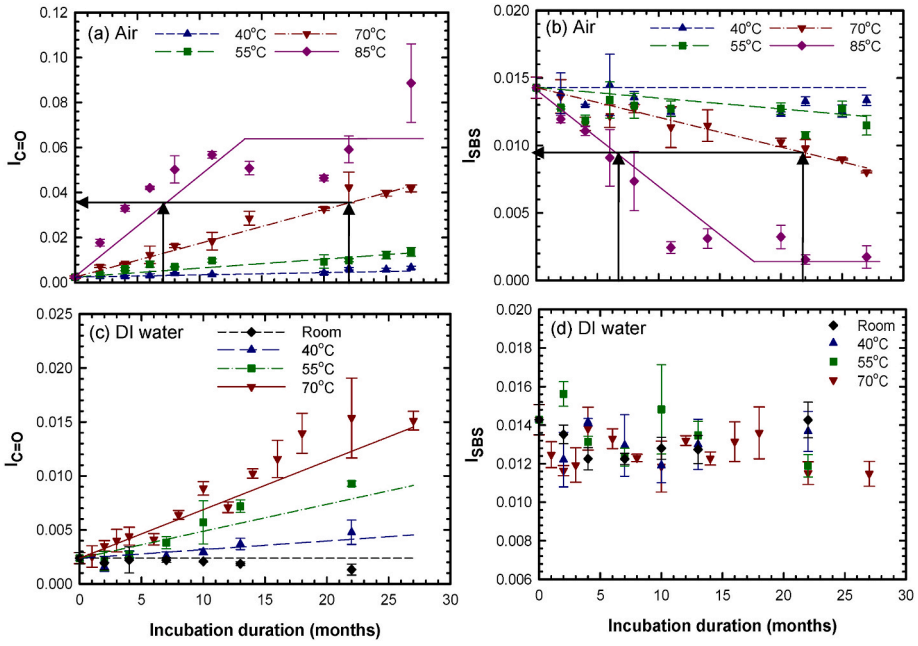

Fig. 13. Variation of the carbonyl and SBS indices with the incubation time of the BGM at different temperatures: (a) $I_{C=O}$ in air; (b) I_{SBS} in air; (c) $I_{C=O}$ in DI water; (d) I_{SBS} in DI water. Arrows represent the values at which the air samples reached brittleness.

of the degradation of the BGM at different field temperatures using time-temperature superposition. Arrhenius modelling is commonly used for establishing predictions for geosynthetics (e.g., Ewais et al., 2018; Hsuan and Koerner 1998; Koerner et al., 1992; Rowe et al., 2020; Rowe and Sangam 2002) and bitumen (e.g., Jin et al., 2011; Lesueur 2009; Mastrofini and Scarsella 2000; Naskar et al., 2012; Rek and Barjaktarović 2002; Wang et al., 2019b) by extrapolating the degradation times in the different properties at temperatures below the accelerated ageing temperatures viz:

$$\ln(s) = \ln(A) - \left(\frac{E_a}{R}\right)\left(\frac{1}{T}\right) \quad \text{(Eq 3)}$$

Where s (month^{-1}) = the degradation rate for a given property, A (month^{-1}) = a constant called a collision factor, E_a (J·mol^{-1}) = the activation energy for the reaction, $R = 8.314$ (J·mol^{-1} K^{-1}) = the universal gas constant, and T (K) = the absolute temperature.

Equation (3) is typically used for uniform/single formulation materials since it is based on the assumption that the kinetics of a reaction is monotonically influenced by temperature (Koerner et al., 1992). Thus, it cannot be used to predict the overall degradation in a multi-component material such as BGMs involving different reaction rates related to the different degradation mechanisms in its different components. However, since the degradation in the mechanical properties is only related to the

NW-GTX component and the chemical and rheological properties were examined for the bitumen coat only, different Arrhenius equations were used to separately establish the degradation rates in these different properties related to these different components of the BGM. These degradation rates were obtained from the slope of the degradation curves (i.e., a BGM property versus the incubation time) at different temperatures for the samples immersed in air and DI water based on the currently available data.

Based on the proposed criterion for defining the nominal failure of BGMs (i.e., either the loss of the viscoelastic characteristics of the bitumen or the degradation in the mechanical properties of the BGM), the tensile ε_{max} was only used to assess the nominal failure based on mechanical properties. This is because ε_{max} showed more sensitivity to the BGM degradation than the maximum tensile strength and hence should result in more conservative estimates of the BGM degradation times. For the bitumen coat, properties such as the T_g, G^*, δ, $I_{C=O}$ and I_{SBS} could be used to establish the time to brittleness of the bitumen coat that define the loss of its viscoelastic characteristics. However, T_g was excluded since it was stabilized at a constant value before brittleness was reached and hence the assessment of the time to brittleness cannot be established based on T_g. I_{SBS} was also excluded because it is only related to the degradation in the SBS copolymer and not the entire bitumen coat. Thus, predictions of the time to brittleness of the bitumen coat were established based on G^* and δ (reflecting the rigidity point at brittleness) and $I_{C=O}$ (inferring the severe oxidative degradation of the bitumen) to reach the values measured experimentally at both 70 and 85 °C when brittleness was first observed in the samples incubated in air (i.e., $G^* =$ 640 kPa, $\delta = 20°$, and $I_{C=O} = 0.035$). Based on these different degradation mechanisms in the BGM components, the time to nominal failure of the BGM was established as the time taken for ε_{max} to reach 50% of the minimum value specified by the BGM manufacturer (i.e., 50% of the specified value; Rowe et al., 2009), that is 33 mm for this BGM (Table 1), and the time to brittleness of the bitumen coat assessed based on G^*, δ, and $I_{C=O}$.

Table 4 shows the degradation rates obtained at different temperatures for ε_{max}, G^*, δ and $I_{C=O}$ that were used to establish the Arrhenius plots for air and DI water immersion (Fig. 14). Except for the ε_{max} and δ in DI water, the Arrhenius plots were established based on three or more temperatures and hence resulted in coefficients of determination (R^2) greater than 0.92 (Fig. 14). With only two data points used in the Arrhenius plots for ε_{max} and δ in DI water, the activation energies were assumed to be similar to those obtained for these two properties in air immersion in which degradation was obtained at three or more temperatures (resulting in $R^2 < 1$ for ε_{max} and δ; Fig. 14b). This approximation was made to allow establishing predictions based on these two properties using the available data. To improve the accuracy of the Arrhenius plot and hence the predictions at lower field temperatures for these two properties, longer incubation is required to obtain the degradation rates at lower experimental temperatures. However, previous studies (e.g., Ewais et al., 2018; Rowe et al., 2020) showed that Arrhenius plots established based only on two elevated temperatures typically result in shorter predictions at lower temperatures than those established using a range of low and high temperatures. This suggests that the current predictions presented herein err on the conservative side.

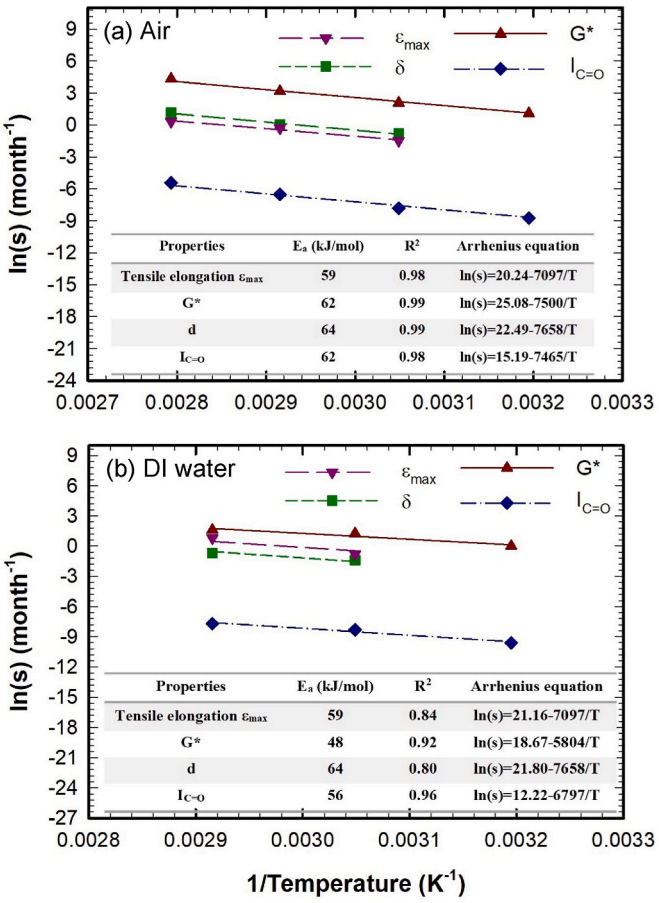

Fig. 14. Arrhenius plots of the elongation at maximum tensile stress (ε_{max}), complex shear modulus (G*), phase angle (δ), and carbonyl index ($I_{C=O}$) for the samples immersed in: (a) air (based on data collected at 40, 55, 70, and 85 °C); and (b) DI water (based on data collected at 22, 40, 55, and 70 °C).

The predictions for the time to nominal failure of the BGM based on both the reduction in ε_{max} to reach 50% of the minimum value specified by the manufacturer and time to brittleness in the bitumen coat at temperatures between 5 and 85 °C in air and DI water are presented in Table 5. In general, predictions based on the tensile ε_{max} were shorter than the time to brittleness in the bitumen coat in DI water while in air, the predictions were longer for ε_{max} than all the other properties at all temperatures. For example, at 10 °C in DI water, the predicted time nominal failure for the BGM based on ε_{max} was 145 years, while the time to brittleness in the bitumen coat ranged between 280 and 360 years based on the G^*, δ and $I_{C=O}$. This shows that in DI water, degradation in

Table 4
Degradation rates of the BGM samples immersed in air and DI water at different temperatures.

Temperature (°C)	Degradation rates for samples incubated in air (month^{-1})[a]				Degradation rates for samples incubated in DI water (month^{-1})[b]			
	ε_{max}	G*	Δ	$I_{C=O}$	ε_{max}	G*	δ	$I_{C=O}$
22	–	–	–	–	NR	NR	NR	NR
40	NR	3.00	NR	0.00016	NR	1.00	NR	0.000068
55	0.23	8.00	0.45	0.00040	0.45	3.50	0.25	0.00025
70	0.75	24.00	1.05	0.0015	2.20	5.00	0.50	0.00045
85	1.40	76.00	3.20	0.0045	–	–	–	–

NR = Degradation in properties was not reached during the current study.
[a] Degradation rates in air were obtained at 40, 55, 70, and 85 °C.
[b] Degradation rates in DI were obtained at 22, 40, 55, and 70 °C.

Table 5
Predicted time to nominal failure of the BGM in years at different temperatures in air and DI water (rounded to two significant digits).

Temperature (°C)	Air immersion				DI water immersion			
	ε_{max}	G*	δ	$I_{C=O}$	ε_{max}	G*	δ	$I_{C=O}$
5	570	**290**	295	315	**230**	400	590	560
10	360	**180**	**180**	200	**145**	280	360	360
20	155	75	**70**	80	**60**	140	140	160
30	70	**30**	**30**	35	**28**	70	60	75
40	35	15	**14**	16	**15**	40	25	35
55	11	4.8	**4.5**	5.2	**4.6**	16	8.8	13
70	4.5	1.8	**1.6**	1.9	**1.8**	7.6	3.2	5.4
85	1.9	0.7	**0.6**	0.8	**0.8**	3.7	1.3	2.4

Numbers in bold show the property governing the time to nominal failure.
For ε_{max}, time to nominal failure was established based on the time to reach 50% of the minimum value (33 mm) specified by the manufacturer for this BGM.
For G*, δ, and $I_{C=O}$, time to nominal failure was established based on the time to brittleness of the bitumen coat when the values reach 620 kPa, 20°, and 0.035, respectively.

the mechanical properties governs the durability of the BGM similar to the experimental data obtained at elevated temperatures. In air, the predictions at 10 °C were 360, 180, 180 and 200 years for ε_{max}, G^*, δ and $I_{C=O}$, respectively, showing that the oxidative degradation of the bitumen governs the longevity of BGMs exposed to air.

4.7. Practical implications of the time to nominal failure of BGMs

The different degradation mechanisms of BGMs involving either the loss of mechanical properties or embrittlement of the bitumen coat may result in reaching the end of their service life in the field. This is because either the rupture of the BGM under the long-term sustained tensile strains in the field due to the degradation in the BGM reinforcement or the potential loss of water tightness due to the brittleness of the bitumen coat may lead to the loss of the hydraulic barrier characteristics of the BGM liner under field conditions. Notwithstanding, the predictions presented in Table 5 for the degradation times in the different properties of the BGM were established based on immersion tests that only examine the changes in the resistance component of the service life of the BGM (i.e., its durability). These experiments do not simulate the demand component (e.g., tensile stresses/strains) on the liner that could induce ruptures/cracking in the aged BGM nor the relaxation of stresses in the BGM that can occur prior to ageing (e.g., Abdelaal et al., 2014a; Rowe et al., 2010). Hence, they should not be treated as predictions of the BGM service life (i.e., time to rupture) in the field. The service life of BGMs in the field can be shorter or potentially much longer than the estimated time to nominal failure presented in Table 5, depending on the demand on the BGM in the field that is a function of many design factors that affect the tensile strains developed in the liner system (Rowe et al., 2020). This is an area where much more research is required since the mechanisms by which BGMs fail in long-term are currently unknown. However, and despite this knowledge gap, these predictions can present a lower bound (i.e., conservative) estimation of the BGM longevity in well designed and constructed liner systems.

While the time to nominal failure presented herein is different from the service life of the liner, it presents a useful evaluation of the relative effect of the variables considered on the BGM material durability. Among these variables that were examined in the current study, the effect of BGM temperature showed a significant effect on its time to nominal failure (either the degradation in the mechanical properties or brittleness in the bitumen coat). For instance, considering the temperature of 6.1–15.3 °C reported by Touze-Foltz and Farcas (2017), the estimated time to nominal failure based on the mechanical properties at an average temperature of 10 °C was 360 years while the estimated time to brittleness was 180–200 years for the BGMs samples exposed to air (Table 5). This is consistent with the findings of Touze-Foltz and Farcas (2017) who did not observe any degradation in mechanical properties of the BGM or loss of water tightness after 30 years of exposure in the field. However, at temperatures of around 85 °C similar to the liner temperature of the exposed BGM examined by Addis et al. (2013) and showed degradation in the mechanical properties after several months from installation, the estimated time to nominal failure ranged between 8 and 23 months based on the different BGM properties (Table 5). With such variation in the degradation times of BGMs with the temperature, the current results highlight the need for considering the expected service temperature of the liner when selecting BGMs for the liner material of geoenvironmental applications with long design lives to ensure adequate environmental protection.

5. Summary and conclusions

The effect of elevated temperatures on the degradation behaviour of a 4.8 mm thick elastomeric BGM immersed in air and DI water was examined at different temperatures using oven immersion tests. The degradation of the BGM mechanical properties was assessed based on the tensile and puncture tests, while degradation in the chemical and rheological properties of the bitumen was assessed using the MDSC, DSR, and FTIR testing techniques. Arrhenius modelling was used to estimate the degradation time in these different properties at different temperatures in air and DI water. Based on the incubation media and the BGM examined herein, the following conclusions were reached:

1. The BGM exhibited different degradation rates in its different components when exposed to elevated temperatures. The extent of degradation in these different components was dependent on the incubation media. To ensure reliable estimates of the long-term performance of BGMs as a hydraulic barrier layer, their degradation behaviour should be assessed based on a holistic investigation of their chemical, mechanical, and rheological properties.
2. In air, exposing the BGM to elevated temperatures resulted in faster degradation of the bitumen coat than in the mechanical properties of the BGM. The degradation in the chemical and rheological properties of the bitumen involved oxidation of the bitumen coat, degradation and consumption of the SBS copolymer, a change in the glass transition temperature, and the increase in the bitumen rigidity with time. While these changes in the bitumen chemical structure did not affect the mechanical strength of the BGM even after the brittleness in the bitumen coat observed at 70 and 85 °C, they resulted in the reduction of the elongation at maximum strength and the ductility of the BGM.
3. In DI water, while the bitumen coat exhibited substantially less degradation in the chemical and rheological properties than in air, it seems that the relatively intact/slightly degraded bitumen coat did not protect the NW-GTX from the degradation by hydrolysis. This is because both the BGM and the NW-GTX that was separately examined in DI water exhibited similar degradation in their mechanical properties. Thus, the degradation in the mechanical properties of the BGM was faster in DI water than in air.
4. Due to the difference in the degradation behaviour of BGMs in different incubation media, time to nominal failure was defined as either the time for the elongation at maximum tensile strength to reach 50% of the minimum values specified by the manufacturer or the time to brittleness of the bitumen coat assessed based on the complex shear modulus, phase angle, and the carbonyl index. This criterion for nominal failure was adopted since the degradation in any of these components of the BGM may lead to the loss of its hydraulic barrier function under the field conditions.
5. Based on Arrhenius modelling, the time to nominal failure varied significantly at field temperatures between 5 and 40 °C. For instance, the estimated time to nominal failure for samples immersed in air based on the tensile elongation ranged from 570 years at 5 °C to 35 years at 40 °C. While these predictions are considered conservative

estimates of the BGM durability established using the double sided immersion tests, they highlight the need for considering the expected liner temperatures in the field when selecting BGMs for the barrier systems of different geoenvironmental applications to ensure adequate environmental protection.

This study allows an assessment of how elevated temperatures and incubation media affect the degradation of an elastomeric BGM. The results are relevant to the particular BGM, and conditions examined. Different results may be expected for other BGMs with different formulations or when other immersion solutions are used. Thus, independent verification is needed before extrapolating the predicted degradation times to other materials and conditions. Furthermore, the predictions presented in this study for DI water were established based on immersion tests involving double-sided exposure of the BGM (i.e., bitumen coat from the top and the polymeric film from the bottom) to solutions that are expected to be more aggressive than field exposure conditions in which the BGM is only exposed to solution from the top surface. Thus, the predictions reported herein are expected to be more conservative estimates (i.e., shorter) for the degradation times than the degradation times in the field. However, the results presented herein provide considerable insight into the degradation behaviour of BGMs at elevated temperatures.

Declaration of competing interest

The authors declare that they have no known competing financial interests or personal relationships that could have appeared to influence the work reported in this paper.

Data availability

Data will be made available on request.

Acknowledgement

The research presented in this paper was funded by the Natural Science and Engineering Research Council of Canada (NSERC) through the Discovery Grant program to F. B. Abdelaal (RGPIN-2018-04091). The equipment used was provided by funding from the Canada Foundation for Innovation (CFI) and the Ontario Ministry of Research Innovation and Science. The authors acknowledge the contribution of Titan Environmental Containment Ltd. for providing the BGM material examined in this study.

References

Abdelaal, F.B., Solanki, R., 2022. Effect of geotextile ageing and geomembrane surface roughness on the geomembrane-geotextile interfaces for heap leaching applications. Geotext. Geomembranes 50 (1), 55–68. https://doi.org/10.1016/j.geotexmem.2021.09.001.

Abdelaal, F.B., Morsy, M.S., Rowe, R.K., 2019. Long-term performance of a HDPE geomembrane stabilized with HALS in chlorinated water. Geotext. Geomembranes 47 (6), 815–830. https://doi.org/10.1016/j.geotexmem.2019.103497.

Abdelaal, F.B., Rowe, R.K., Brachman, R.W.I., 2014a. Brittle rupture of an aged HDPE geomembrane at local gravel indentations under simulated field conditions. Geosynth. Int. 21 (1), 1–23. https://doi.org/10.1680/gein.13.00031.

Abdelaal, F.B., Rowe, R.K., Islam, M.Z., 2014b. Effect of leachate composition on the long-term performance of a HDPE geomembrane. Geotext. Geomembranes 42, 348–362. https://doi.org/10.1016/j.geotexmem.2014.06.001.

Addis, P., Andruchow, B., Wislesky, I., 2013. In: Bituminous Geomembrane Failure at a Co-disposal Tailings Storage Facility. Publisher: University of Alberta, Edmonton, Alberta, Canada. *Proceeding Of the 17th International Conference On Tailings And Mine Waste*, Banff, AB, Canada, pp. 457–466. https://doi.org/10.7939/r3-ds53-4h45.

Aguiar-Moya, J.P., Salazar-Delgado, J., García, A., Baldi-Sevilla, A., Bonilla-Mora, V., Loría-Salazar, L.G., 2017. Effect of ageing on micromechanical properties of bitumen by means of atomic force microscop. Road Mater. Pavement Des. 18 (Suppl. 2), 203–215. https://doi.org/10.1080/14680629.2017.1304249.

Airey, G., 2003. Rheological properties of styrene butadiene styrene polymer modified road bitumens. Fuel 82 (14), 1709–1719. https://doi.org/10.1016/S0016-2361(03)00146-7.

Arias, G.K.B., 2019. Influence of Oxidative Aging on the Chemistry and Rheology of Asphalt Cement from Bolivian, Canadian and Costa Rican Sources. Thesis (Ph.D.). Queen's University (Canada). https://qspace.library.queensu.ca/handle/1974/26072.

Aske, N., Kallevik, H., Sjöblom, J., 2001. Determination of saturate, aromatic, resin, and asphaltenic (SARA) components in crude oils by means of infrared and near-infrared spectroscopy. Energy Fuel. 15 (5), 1304–1312. https://doi.org/10.1021/ef010088h.

ASTM D4833/D4833M. Standard Test Method for Index Puncture Resistance of Geomembranes and Related Products. American Society for Testing and Materials, West Conshohocken, Pennsylvania, USA.

ASTM D5035. Standard Test Method for Breaking Force and Elongation of Textile Fabrics (Strip Method). American Society for Testing and Materials, West Conshohocken, Pennsylvania, USA.

ASTM D5199. Standard Test Method for Measuring the Nominal Thickness of Geosynthetics". American Society for Testing and Materials, West Conshohocken, Pennsylvania, USA.

ASTM D5261. Standard Test Method for Measuring Mass Per Unit Area of Geotextiles". American Society for Testing and Materials, West Conshohocken, Pennsylvania, USA.

ASTM D7275. Standard Test Method for Tensile Properties of Bituminous Geomembranes (BGM). American Society for Testing and Materials, West Conshohocken, Pennsylvania, USA.

ASTM E2602. Standard Test Methods for the Assignment of the Glass Transition Temperature by Modulated Temperature Differential Scanning Calorimetry. American Society for Testing and Materials, West Conshohocken, Pennsylvania, USA.

Bachir, D.S., Dekhli, S., Mokhtar, K.A., 2016. Rheological evaluation of ageing properties of SEBS polymer modified bitumens. Period. Polytech. Civ. Eng. 60 (3), 397–404. https://doi.org/10.3311/PPci.7853.

Bannour, H., Barral, C., Touze-Foltz, N., 2013. Flow rate in composite liners including GCLs and a bituminous geomembrane. In: Frikha, W. (Ed.), Proceedings of the 3rd International Conference on Geotechnical Engineering, S5–9, pp. 809–819. Hamamet, Tunisia.

Benefield, L., Judkins, J., Weand, B., 1982. Process Chemistry for Water and Wastewater Treatment. Prentice Hall, Englewood Cliffs, NJ.

Cazzuffi, D., Gioffrè, D., 2020. Lifetime assessment of exposed PVC-P geomembranes installed on Italian dams. Geotext. Geomembranes 48, 130–136. https://doi.org/10.1016/j.geotexmem.2019.11.015.

Corbett, L.W., 1969. Composition of asphalt based on generic fractionation, using solvent deasphaltening, elution-adsorption chromatography, and densimetric characterization. Anal. Chem. 41 (4), 576–579. https://doi.org/10.1021/ac60273a004.

Daly, N., Breul, B., 2017. Exceptional longevity of bituminous geomembrane through several decades of practice. In: Proceedings of 70th Canadian Geotechnical Conference, Ottawa, Canada. Publisher: Canadian Geotechnical Society, Surrey, BC, Canada, p. 7.

Dealy, J.M., 1979. Rheological properties of oil sand bitumens. Can. J. Chem. Eng. 57 (6), 677–683. https://doi.org/10.1002/cjce.5450570604.

Ding, Y., Li, D., Zhang, H., Deng, M., Mao, X., Cao, X., 2022. Investigation of aging behavior of asphalt under multiple environmental conditions. J. Mater. Civ. Eng. 34 (2), 04021419 https://doi.org/10.1061/(ASCE)MT.1943-5533.0004048.

Dumitru, F., Moncea, M., Panait, A., Olteanu, M., Laslo, L., 2017. Laboratory performance testing of two types of geotextiles used in danube hydrotechnical works. In: IOP Conference Series: Materials Science and Engineering, vol. 209. IOP Publishing Ltd, 012101. https://doi.org/10.1088/1757-899X/209/1/012101, 1.

Durrieu, F., Farcas, F., Mouillet, V., 2007. The influence of UV aging of a Styrene/Butadiene/Styrene modified bitumen: comparison between laboratory and on site aging. Fuel 86 (10–11), 1446–1451. https://doi.org/10.1016/j.fuel.2006.11.024.

Eldesouky, H., Brachman, R., 2020. Viscoplastic modelling of HDPE geomembrane local stresses and strains. Geotext. Geomembranes 48, 41–51. https://doi.org/10.1016/j.geotexmem.2019.103503.

Elias, V., Salman, A., Goulias, D., 1998. The effect of pH, resin properties, and manufacturing process on laboratory degradation of polyester geosynthetics. Geosynth. Int. 5 (5), 459–490. https://doi.org/10.1680/gein.5.0133.

Ewais, A.M.R., Rowe, R.K., Scheirs, J., 2014. Degradation behaviour of HDPE geomembranes with high and low initial high-pressure oxidative induction time. Geotext. Geomembranes 42 (2), 111–126. https://doi.org/10.1016/j.geotexmem.2014.01.004.

Ewais, A.M.R., Rowe, R.K., Rimal, S., Sangam, H.P., 2018. 17-year elevated temperature study of HDPE geomembrane longevity in air, water and leachate. Geosynth. Int. 25 (5), 525–544. https://doi.org/10.1680/jgein.18.00016.

Fernández-Gómez, W.D., Quintana, H.a.R., Daza, C.E., Lizcano, F.a.R., 2014. The effects of environmental aging on Colombian asphalts. Fuel 115, 321–328. https://doi.org/10.1016/j.fuel.2013.07.009.

GRI-GM13, 2021. Standard Specification for Test Properties, Testing Frequency and Recommended Warrant for High Density Polyethylene (HDPE) Smooth and Textured Geomembranes, Rev, vol. 6. Geosynthetics Research Institute, USA.

Hofko, B., Cannone Falchetto, A., Grenfell, J., Huber, L., Lu, X., Porot, L., Poulikakos, L., You, Z., 2017. Effect of short-term ageing temperature on bitumen properties. Road Mater. Pavement Des. 18 (Suppl. 2), 108–117. https://doi.org/10.1080/14680629.2017.1304268.

Hsuan, Y., Koerner, R., 1998. Antioxidant depletion lifetime in high density polyethylene geomembranes. J. Geotech. Geoenviron. Eng. 124 (6), 532–541. https://doi.org/10.1061/(ASCE)1090-0241(1998)124:6(532).

Hunter, R.N., Self, A., Read, J., 2015. The Shell Bitumen Handbook. ICE Publishing, London, UK.

Jin, X., Han, R., Cui, Y., Glover, C.J., 2011. Fast-rate–constant-rate oxidation kinetics model for asphalt binders. Ind. Eng. Chem. Res. 50 (23), 13373–13379. https://doi.org/10.1021/ie201275q.

Jing, R., Varveri, A., Liu, X., Scarpas, A., Erkens, S., 2019. Laboratory and field aging effect on bitumen chemistry and rheology in porous asphalt mixture. Transport. Res. Rec. 2673 (3), 365–374 https://doi.org/10.1177%2F0361198119833362.

Kaya, D., Topal, A., Gupta, J., Mcnally, T., 2020. Aging effects on the composition and thermal properties of styrene-butadiene-styrene (SBS) modified bitumen. Construct. Build. Mater. 235, 117450 https://doi.org/10.1016/j.conbuildmat.2019.117450.

Koerner, R.M., Lord, A.E., Hsuan, Y.H., 1992. Arrhenius modeling to predict geosynthetic degradation. Geotext. Geomembranes 11 (2), 151–183. https://doi.org/10.1016/0266-1144(92)90042-9.

Kriz, P., Stastna, J., Zanzotto, L., 2007. Effect of low-temperature isothermal conditioning on glass transition in asphalt binders, 2007. In: *Proceedings Of the 52nd Annual Conference-Canadian Technical Asphalt Association (CTAA)*, Niagara Falls, ON, Canada, vol. 52. Polyscience Publications, Laval, Quebec, Canada, 159–84.

Lamontagne, J., Dumas, P., Mouillet, V., Kister, J., 2001. Comparison by fourier transform infrared (FTIR) spectroscopy of different ageing techniques: application to road bitumens. Fuel 80 (4), 483–488. https://doi.org/10.1016/S0016-2361(00)00121-6.

Lazaro, J., Breul, B., 2014. Bituminous geomembrane in heap leach pads. In: Proceedings of Heap Leach Solutions, Lima, Peru. InfoMine Inc., Canada, pp. 291–303.

Lesueur, D., 2009. The colloidal structure of bitumen: consequences on the rheology and on the mechanisms of bitumen modification. Adv. Colloid Interface Sci. 145 (1–2), 42–82. https://doi.org/10.1016/j.cis.2008.08.011.

Liu, K., Xu, G., Voyer, R., 2003. Durability and cold temperature performance of SBS-modified bituminous roofing membranes. In: Wallace, T.J. (Ed.), *Roofing Research And Standards Development: 5th Volume*. ASTM STP 145, W. J. Rossiter. ASTM International, West Conshohocken, PA. https://doi.org/10.1520/stp11453s.

Lu, X., Isacsson, U., 2002. Effect of ageing on bitumen chemistry and rheology. Construct. Build. Mater. 16 (1), 15–22. https://doi.org/10.1016/S0950-0618(01)00033-2.

Lu, X., Talon, Y., Redelius, P., 2008. Ageing of bituminous binders - laboratory tests and field data. In: Proceedings of the 4th Eurasphalt & Eurobitume Congress. European Asphalt Pavement Association (EAPA), Copenhagen. Denmark, pp. 21–23.

Mark, J., Ngai, K., Graessley, W., Mandelkern, L., Samulski, E., Koenig, J., Wignall, G., 2004. The Glass Transition and the Glassy State. Physical Properties of Polymers, 3 ed. Cambridge University Press, Cambridge, pp. 72–152.

Masson, J.F., Polomark, G.M., 2001. Bitumen microstructure by modulated differential scanning calorimetry. Thermochim. Acta 374 (2), 105–114. https://doi.org/10.1016/S0040-6031(01)00478-6.

Mastrofini, D., Scarsella, M., 2000. The application of rheology to the evaluation of bitumen ageing. Fuel 79 (9), 1005–1015. https://doi.org/10.1016/S0016-2361(99)00244-6.

Mathur, A., Netravali, A.N., O'rourke, T.D., 1994. Chemical aging effects on the physio-mechanical properties of polyester and polypropylene geotextiles. Geotext. Geomembranes 13, 591–626. https://doi.org/10.1016/0266-1144(94)90012-4.

Marcotte, B.A., Fleming, I.R., 2020. Damage to geomembrane liners from tire derived aggregate. Geotext. Geomembranes 48 (2), 198–209. https://doi.org/10.1016/j.geotexmem.2019.11.005.

Mckay, J., Amend, P., Cogswell, T., Harnsberger, P., Erickson, R., Latham, D., 1978. Petroleum asphaltenes: chemistry and composition. In: Uden, P.C., Siggia, S., Jensen, H.B. (Eds.), *Analytical Chemistry Of Liquid Fuel Sources*; Tar Sands, Oil Shale, Coal, and Petroleum. American Chemical Society, Washington DC, pp. 128–142. https://doi.org/10.1021/ba-1978-0170.ch009, 1978.

Mirwald, J., Werkovits, S., Camargo, I., Maschauer, D., Hofko, B., Grothe, H., 2020. Understanding bitumen ageing by investigation of its polarity fractions. Construct. Build. Mater. 250, 118809 https://doi.org/10.1016/j.conbuildmat.2020.118809.

Mouillet, V., Farcas, F., Besson, S., 2008. Ageing by UV radiation of an elastomer modified bitumen. Fuel 87 (12), 2408–2419. https://doi.org/10.1016/j.fuel.2008.02.008.

Mouillet, V., Farcas, F., Chailleux, E., 2011. Physico-chemical techniques for analysing the ageing of polymer modified bitumen. In: Chapter 12, Polymer Modified Bitumen: Properties And Characterisation. Tony McNally, Woodhead Publishing Limited, Cambridge, UK, pp. 366–395. https://doi.org/10.1533/9780857093721.2.366.

Müller, Werner, 2007. HDPE geomembranes in geotechnics. Springer-Verlag Berlin Heielberg, Berlin, Germany.

Müller, W., Jacob, I., 2003. Oxidative resistance of high density polyethylene geomembranes. Polym. Degrad. Stabil. 79 (No. 1), 161–172. https://doi.org/10.1016/S0141-3910(02)00269-0.

Naskar, M., Reddy, K.S., Chaki, T.K., Divya, M.K., Deshpande, A.P., 2012. Effect of ageing on different modified bituminous binders: comparison between RTFOT and radiation ageing. Mater. Struct. 46 (7), 1227–1241. https://doi.org/10.1617/s11527-012-9966-3.

Ojovan, M.I., 2008. Configurons: thermodynamic parameters and symmetry changes at glass transition. Entropy 10 (3), 334–364. https://doi.org/10.3390/e10030334.

Omairey, E.L., Zhang, Y., Gu, F., Ma, T., Hu, P., Luo, R., 2020. Rheological and fatigue characterisation of bitumen modified by anti-ageing compounds. Construct. Build. Mater. 265, 120307 https://doi.org/10.1016/j.conbuildmat.2020.120307.

Peggs, I., 2008. Prefabricated bituminous geomembrane: a candidate for exposed geomembrane caps for landfill closures. In: Proceedings of the First Pan American Geosynthetics Conference and Exhibition, Cancun, Mexico. Industrial Fabrics Association International (IFAI), USA, pp. 191–197.

Petersen, J.C., 1998. A dual, sequential mechanism for the oxidation of petroleum asphalts. Petrol. Sci. Technol. 16 (9–10), 1023–1059. https://doi.org/10.1080/10916469808949823.

Puello, J., Afanasjeva, N., Alvarez, M., 2013. Thermal properties and chemical composition of bituminous materials exposed to accelerated ageing. Road Mater. Pavement Des. 14 (2), 278–288. https://doi.org/10.1080/14680629.2013.785799.

Rek, V., Barjaktarović, Z.M., 2002. Dynamic mechanical behavior of polymer modified bitumen. Mater. Res. Innovat. 6 (2), 39–43. https://doi.org/10.1007/s10019-002-0159-5.

Rowe, R.K., Fan, J., 2021. Effect of geomembrane hole geometry on leakage overlain by saturated tailings. Geotext. Geomembranes 49 (6), 1506–1518.

Rowe, R.K., Fan, J., 2022. A general solution for leakage through geomembrane defects overlain by saturated tailings and underlain by highly permeable subgrade. Geotext. Geomembranes 50 (4), 694–707. https://doi.org/10.1016/j.geotexmem.2022.03.010.

Rowe, R.K., Ewais, A.M.R., 2014. Antioxidant depletion from five geomembranes of same resin but of different thicknesses immersed in leachate. Geotext. Geomembranes 42, 540–554. https://doi.org/10.1016/j.geotexmem.2014.08.001.

Rowe, R.K., Sangam, H.P., 2002. Durability of HDPE geomembranes. Geotext. Geomembranes 20 (2), 77–95. https://doi.org/10.1016/S0266-1144(02)00005-5.

Rowe, R.K., Abdelaal, F., Zafari, M., Morsy, M., Priyanto, D., 2020. An approach to high-density polyethylene (HDPE) geomembrane selection for challenging design requirements. Can. Geotech. J. 57 (10), 1550–1565. https://doi.org/10.1139/cgj-2019-0572.

Rowe, R.K., Rimal, S., Sangam, H.P., 2009. Ageing of HDPE geomembrane exposed to air, water and leachate at different temperatures. Geotext. Geomembranes 27 (2), 131–151. https://doi.org/10.1016/j.geotexmem.2008.09.007.

Rowe, R.K., Islam, M.Z., Brachman, R.W.I., Arnepalli, D.N., Ewais, A., 2010. Antioxidant depletion from an HDPE geomembrane under simulated landfill conditions. ASCE J. Geotech. Geoenviron. Eng. 136 (7), 930–939. https://doi.org/10.1061/(ASCE)GT.1943-5606.0000302.

Samea, A., Abdelaal, F.B., 2019. Chemical durability of bituminous geomembranes in heap leaching applications at 55°C. In: Proceedings of Geosynthetics 2019 Conference, Houston, Texas, USA. Industrial Fabrics Association International (IFAI), USA, pp. 298–308.

Scheirs, J., 2009. A Guide to Polymeric Geomembranes: a Practical Approach. John Wiley & Sons, West Sussex, United Kingdom.

Stark, T.D., Hernandez, M.A., Rohe, D.S., 2020. Geomembrane factory and field thermally welded seams comparison. Geotext. Geomembranes 48 (4), 454–467. https://doi.org/10.1016/j.geotexmem.2020.02.004.

Sultana, S., Bhasin, A., 2014. Effect of chemical composition on rheology and mechanical properties of asphalt binder. Construct. Build. Mater. 72, 293–300. https://doi.org/10.1016/j.conbuildmat.2014.09.022.

Tauste, R., Moreno-Navarro, F., Sol-Sánchez, M., Rubio-Gámez, M., 2018. Understanding the bitumen ageing phenomenon: a review. Construct. Build. Mater. 192, 593–609. https://doi.org/10.1016/j.conbuildmat.2018.10.169.

Tian, K., Benson, C.H., Yang, Y., Tinjum, J.M., 2018. Radiation dose and antioxidant depletion in a HDPE geomembrane. Geotext. Geomembranes 46, 426–435. https://doi.org/10.1016/j.geotexmem.2018.03.003.

Touze-Foltz, N., Xie, H., Stoltz, G., 2021. Performance issues of barrier systems for landfills: a review. Geotext. Geomembranes 49 (2), 475–488. https://doi.org/10.1016/j.geotexmem.2020.10.016.

Touze-Foltz, N., Farcas, F., 2017. Long-term performance and binder chemical structure evolution of elastomeric bituminous geomembranes. Geotext. Geomembranes 45 (2), 121–130. https://doi.org/10.1016/j.geotexmem.2017.01.003.

Vahidi, S., Hsuan, G., Elsafty, A., 2020. Predicting the depletion of antioxidants in high density polyethylene (HDPE) under sunlight using the reciprocity law. Geotext. Geomembranes 48, 170–175. https://doi.org/10.1016/j.geotexmem.2019.11.009.

Verdonck, E., 2010. Characterization of Bitumen by Modulated Differential Scanning Calorimetry and High Resolution Thermogravimetric Analysis. Zellik, Belgium. TA Instruments-Waters LLC, 6pp. Accessed online October 2022: https://www.tainstruments.com/pdf/literature/TA377%20Characterization%20of%20Bitumen%20by%20MDSC%20and%20High%20Resolution%20Thermogravimetry.pdf.

Wang, D., Liu, Q., Yang, Q., Tovar, C., Tan, Y., Oeser, M., 2019a. Thermal oxidative and ultraviolet ageing behaviour of nano-montmorillonite modified bitumen. Road Mater. Pavement Des. 22 (1), 121–139. https://doi.org/10.1080/14680629.2019.1619619.

Wang, J., Wang, T., Hou, X., Xiao, F., 2019b. Modelling of rheological and chemical properties of asphalt binder considering SARA fraction. Fuel 238, 320–330. https://doi.org/10.1016/j.fuel.2018.10.126.

Yu, X., Burnham, N.A., Granados-Focil, S., Tao, M., 2019. Bitumen's microstructures are correlated with its bulk thermal and rheological properties. Fuel 254, 115509. https://doi.org/10.1016/j.fuel.2019.05.092.

Yu, X., Zaumanis, M., Dos Santos, S., Poulikakos, L.D., 2014. Rheological, microscopic, and chemical characterization of the rejuvenating effect on asphalt binders. Fuel 135, 162–171. https://doi.org/10.1016/j.fuel.2014.06.038.

Zeng, W., Wu, S., Wen, J., Chen, Z., 2015. The temperature effects in aging index of asphalt during UV aging process. Construct. Build. Mater. 93, 1125–1131. https://doi.org/10.1016/j.conbuildmat.2015.05.022.

Zhang, Y., Wei, H., Dai, Y., 2020. Influence of different aging environments on rheological behavior and structural properties of rubber asphalt. Materials 13 (15), 3376. https://doi.org/10.3390/ma13153376.